Machado, Miguel A.; Antin, Kim Niklas; Rosado, Luís S.; Vilaça, Pedro; Santos, Telmo G.

Contactless high-speed eddy current inspection of unidirectional carbon fiber reinforced polymer

Published in:
Composites Part B: Engineering

DOI:
10.1016/j.compositesb.2018.12.021

Published: 01/07/2019

Document Version
Peer-reviewed accepted author manuscript, also known as Final accepted manuscript or Post-print

Contactless high-speed eddy current inspection of unidirectional carbon fiber reinforced polymer

Miguel A. Machado[a,1], Kim-Niklas Antin[b], Luís S. Rosado[c], Pedro Vilaça[b], Telmo G. Santos[a]

[a] *UNIDEMI, Department of Mechanical and Industrial Engineering, NOVA School of Science and Technology, NOVA University Lisbon, 2829-516 Caparica, Portugal.*
[b] *Department of Mechanical Engineering, School of Engineering, Aalto University, Puumiehenkuja 3, 02150 Espoo, Finland.*
[c] *Instituto Superior Técnico, Universidade de Lisboa, Lisbon, Portugal*
[1] Corresponding author: *p111094@campus.fct.unl.pt*

Abstract

This paper presents the development and the results of a customized eddy current (EC) non-destructive testing (NDT) system for highly demanding online inspection conditions. Several planar eddy current array probes were designed, numerically simulated and experimentally compared for the inspection of low conductivity unidirectional carbon fibre reinforced polymer (CFRP) ropes. The inspections were performed using a dedicated scanner device at 4 m/s with 3 mm probe lift-off where defects under 1 mm were detected with an excellent SNR. Different defect morphologies and sizes, such as broken fibres and lateral cuts, were successful detected and compared to conventional probes.

Keywords: Carbon fiber reinforced polymer; Eddy current testing; Planar probe; High speed; Contactless.

1. Introduction

Unidirectional carbon fibre reinforced polymer composites (UD CFRP) are high performance materials for structural components, however, they exhibit low damage tolerance [1,2]. Condition monitoring is therefore required in safety-critical applications. Several methods for online monitoring of UD CFRP have been suggested. Contact ultrasonic testing provides damage location and morphology [3], but online monitoring is not viable at high speed, due to coupling issues, inadmissibility of component wetting or insufficient sampling rate. Radiography is a contactless alternative to damage localization and characterization, but even when radiation hazard issues are not prohibitive, it typically needs long exposure times [4], compromising high speed inspection. Thermo-elastic stress analysis is faster, but it does not penetrate protective surface coatings, limiting the inspection to the coating. Damage can be detected by observing the surface with optical methods [5,6], but they require a contrast pattern. Similarly, optical fibres can be used to observe local changes in strain [7], but they need to be embedded in the structure. Far field microwave NDE using time reversal mirror has been done with GFRP and metal-composites in 150 × 150 mm samples where disbonding defects, drilled holes and impact damage have been detected [8]. It can be performed without contact, but measurements require 10 minutes and CFRP has not been tested yet. Electric based methods, on the other hand, can use the conductivity of the carbon fibres themselves for damage detection. Resistance [9] and capacitance [10] monitoring can be used to detect strain, fibre breaks and even matrix damage [11,12]. However, resistance measurements do not provide information about the damage location nor morphology.

In contrast, local and contactless electromagnetic methods can be conducted using eddy current testing (ECT). ECT can be used in several ways to inspect carbon fibre composites [13]. It is typically used for inspecting undulations in carbon fibre reinforcement fabrics, quality control of stacking sequence, fibre orientation and curing effects [14–16]. Electrical properties can be characterized through various orientations with ECT techniques [17,18]. Delamination detection has been proposed [19] and shown with artificial delamination made with interply release film [20] and extensive delamination during tension testing [21]. Matrix cracking could be observed using electromagnetic methods if the matrix is made conductive by adding carbon nanotubes [22,23]. Like embedded sensors, this approach may be difficult to implement into existing products and production lines. Artificial cracks made by slitting the fabric before lamination have been detected as well as impact damage [24,25]. Planar ECT probes have demonstrated a superior sensitivity in the detection of imperfections in other low conductivity materials [26–28].

Velocity effects on eddy current (EC) have been demonstrated in specimens with simple shapes, such as, bars, tubes, and wires which are moving [29]. Very low frequencies were simulated (40 Hz) and speeds up to 1000 m/s [30]. The higher the employed frequency, the smaller the speed effect is. For instance, assuming an inspection speed of 4 m/s, the travelled distance during one cycle of 1 MHz ECT is 4 µm, far less than the sensitive area of any practical probe, leaving valid a stationary assumption. Beside this, it is only required that the demodulation of ECT signals is accomplished with enough bandwidth to accommodate for the defect signals. The bandwidth required can be assumed the inverse of the time required for a given test location to travel across the employed probe. As an example, for the same inspection speed, the required bandwidth using a 4 mm sensitive area probe is roughly 1 kHz. In other ECT methods velocity can even be a beneficial factor [31].

There is a growing demand for non-destructive testing techniques for inline condition monitoring of CFRP ropes. Static techniques are insufficient since these ropes can be in movement, or even at high speeds, for example in hoisting applications. The sensors coupling is also crucial since the contact between the probe and the CFRP can damage the elements [32].

There are commercially available solutions [33] especially designed for the non-contact and continuous testing of carbon fibre rovings. The testing system utilizes the electrical conductivity of the carbon fibres to gain information such uniformity of the carbon fibre tow or yarn [34]. However, the present study presents significant differences, since it consists on the condition monitoring of the CFRP in operation, and the fibres are covered by a polymeric coating of about 1 mm thickness, increasing the EC probe lift-off.

This paper presents new EC array probes for NDT inspection of a UD CFRP rope, which is highly demanding task due to high lift-off required, high velocity (up to 4 m/s) and highly anisotropic low conductive composite material. The proposed new EC probes are not limited to this specific inspection tasks, but the results can be extrapolated for other unidirectional CFRP materials.

2. Carbon Fibre Reinforced Polymer Rope

2.1. Material characterization

The carbon fibre rope target in this study is a structural system consisting of four pultruded unidirectional (UD) CFRP elements protected by a polyurethane coating with an average thickness of about 1 mm (**Fig. 1**). Each load carrying CFRP element has a cross section dimension of about 5.0 mm × 2.5 mm. The CFRP elements are pultruded composite rods consisting of carbon fibre reinforcement embedded in an epoxy matrix and aligned along the Z-direction. As the rods are manufactured using a pultrusion line, they are not laminates and do not consist of plies like most CFRP structures. However, they behave in a similar manner as UD laminates. Like laminated structures, the microstructure of the pultruded rods contains resin rich zones, but their orientation varies.

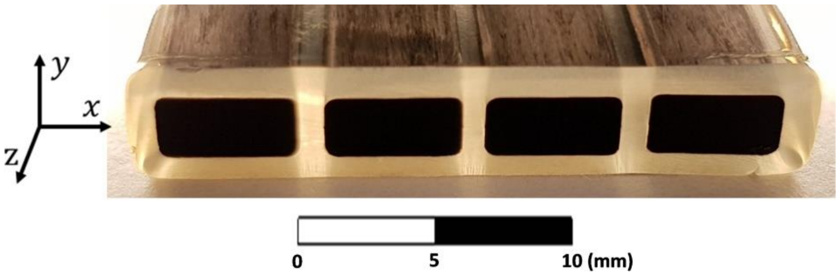

Fig. 1. Cross-section of the CFRP evidencing the four elements with 5 × 2.5 mm cross-section and the polyurethane coating with about 1 mm thickness.

The electrical conductivity σ [S/m] of the elements was measured using different methods. It is the reciprocal of electrical resistivity ρ [Ω.m], according to the equation σ =1/ρ, and its relation with the electrical field $\vec{E}$ [V/m] and the current density $\vec{J}$ [A/m^2] is given by **Eq. 1**. Since $\vec{E}$ and $\vec{J}$ are vectors, ρ is, in general, a tensor. Meaning that the current does not necessary flow in the same direction as the applied electric field [35].

$$\vec{E} = \rho \cdot \vec{J} \qquad \textbf{Eq. 1}$$

The resistivity of the elements was measured along three perpendicular directions (XYZ) represented in **Fig. 2**, using two redundant methods: locally measurement, using a collinear four-point probe (potential drop measurement); and bulk measurement, through two contacts on both ends of a sample, applying Pouillet's law - in this case four-point measurements were performed using a four point probe with four tungsten carbide needles, arranged along a straight line and spaced 0.635 mm, d [m], from each other, A current source forced a constant electrical current I [A] through the external needles. A 2182A nanovoltmeter simultaneously measured the voltage V [V] produced between the inner needles. Assuming an equally-spaced contact points the resistivity of a bulk material (semi-infinite in lateral dimension and with t>>d) is given by **Eq. 2**.

$$\rho = 2 \cdot \pi \cdot d \cdot \frac{V}{I} \qquad \textbf{Eq. 2}$$

The mean tensor of the electrical conductivity is represented by **Eq. 3**. It should be noted that the tensor is diagonal because the XYZ coordinate system corresponds to the principal directions of the tensor (eigenvectors). Therefore, the electrical conductivity along those axes corresponds to the extreme maximum and minimum values (eigenvalues). As expected, the electrical bulk conductivity in the longitudinal direction (Z) is much higher than in X and Y directions, since this is the alignment direction of the fibres. This result shows the high electrical anisotropy of the material, and it was taken into consideration during ECT probe design.

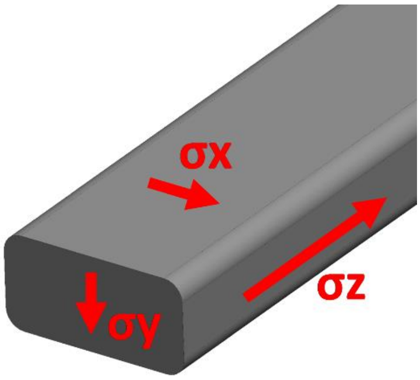

Fig. 2. Directions used to measure the electrical conductivity of the CFRP element.

$$\sigma_{ij} = \begin{bmatrix} \sigma_{xx} & 0 & 0 \\ 0 & \sigma_{yy} & 0 \\ 0 & 0 & \sigma_{zz} \end{bmatrix} = \begin{bmatrix} 117 & 0 & 0 \\ 0 & 78.1 & 0 \\ 0 & 0 & 13000 \end{bmatrix} [{}^{S}/_{m}] \qquad \textbf{Eq. 3}$$

Numerical simulation was performed in order to evaluate the behaviour of EC in the anisotropic CFRP material. For this, the ANSYS Electronics software was used, and it calculates an approximate numerical solution of Maxwell's equations in their full formulation.

Due to the nature of the method, ECT will only be able to inspect the conductive part of the composite system, i.e. the CFRP elements, not being affected by the polymer coating. Therefore, the model used for the simulation comprises of only one carbon fibre element and the probe. The simulated CFRP element has the same section as the specimens, 5 × 2.5 mm, and 100 mm length. A coil was placed 3 mm above the CFRP element. The protective polyurethane coating, invisible to EC, has 1 mm thickness. An additional lift-off of 2 mm was added between the probe and the component to assure a contactless inspection. The total effective lift-off is therefore 3 mm. Different excitation directions were simulated to understand its influence on the EC path under this electrically anisotropic material.

Fig. 3 shows the EC density in the CFRP elements when different unidirectional excitation orientations were considered. Four loops are created in the edges of the CFRP element and away from the excitation when a transversal excitation is used (**Fig. 3a**). By applying a small angle (5°) between Z-direction and the unidirectional excitation (**Fig. 3b**), it is possible to observe a preferred flow direction which is the most conductive direction (Z direction) of the CFRP element. Increasing the angle will facilitate the current flow as depicted. These results were important to determine the preferred probe geometry. A transversal excitation (90º) should be avoided and a longitudinal direction preferred, so a 45° parallelogram coil with only 0º and 45° segments fulfils these conditions best. A pair of 45° parallelogram coils avoids undesired transversal excitation and creates a known output signal when working in bridge differential mode.

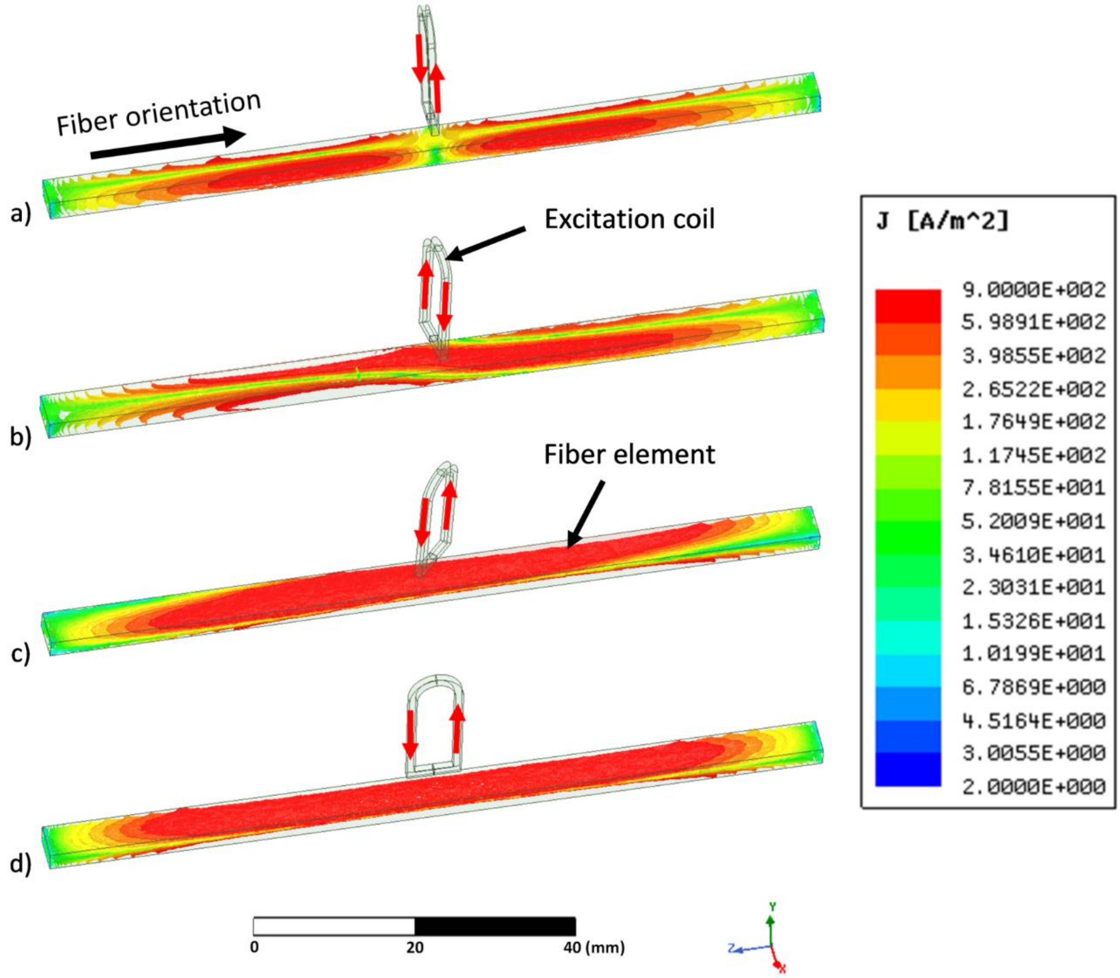

Fig. 3. Current density in an anisotropic material (CFRP) with different excitation orientations: a) Excitation at 90^0 ; b) Excitation at 85^0 ; c) Excitation at 45^0 ; d) Excitation at 0^0 .

2.2.Defect characterization

Defects were induced in the samples by machining and mechanical loading. **Table 1** describes the defects created for each of the four CFRP samples. The defects position along Z direction corresponds to the ones presented in **Fig. 4**, in the same element of the CFRP. Natural defects in this application can be very much alike the artificial ones. Damage can occur on the transport, assembly and use and that damage can be originated by objects falling over the CFRP (similar to broken fibres induced by ball-peen hammering) or some object that gets between the CFRP and the pulley (similar to 3-point bending). The CFRP are tensioned so fibre breaks will show the clear separation which makes cutting the fibres artificially a very close comparation.

Table 1. Machined and real defects in the four CFRP samples.

Defect	Type of defect	Picture	Defect	Type of defect	Picture
LC05	Lateral Cut 0.5 mm length of width	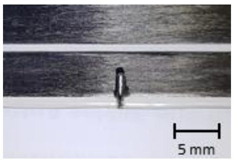	3PTB	Broken fibres or Delamination induced by 3 ptb	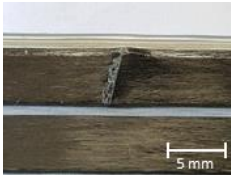
TC05	Cross Top Cut 0.5 mm depth of thickness	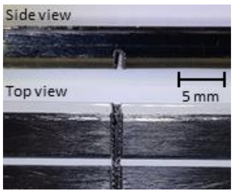	LC02	Lateral Cut 0.2 mm length of width)	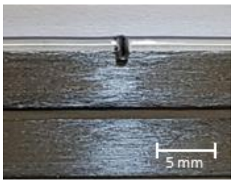
TH05	Top Hole 0.5 mm depth of thickness		LC05	Lateral Cut 0.5 mm length of width	
SH2	Side Hole 2 mm depth	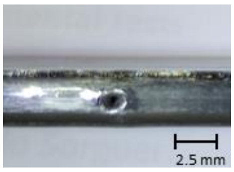	BFH	Broken fibres induced by ball-peen hammering	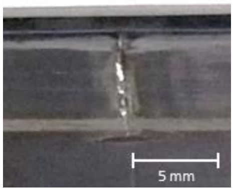
BFH	Broken fibres induced by ball-peen hammering	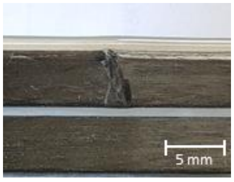	LC025	Lateral Cut 0.25 mm length of width	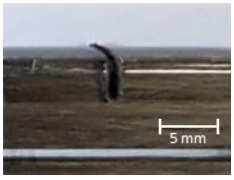

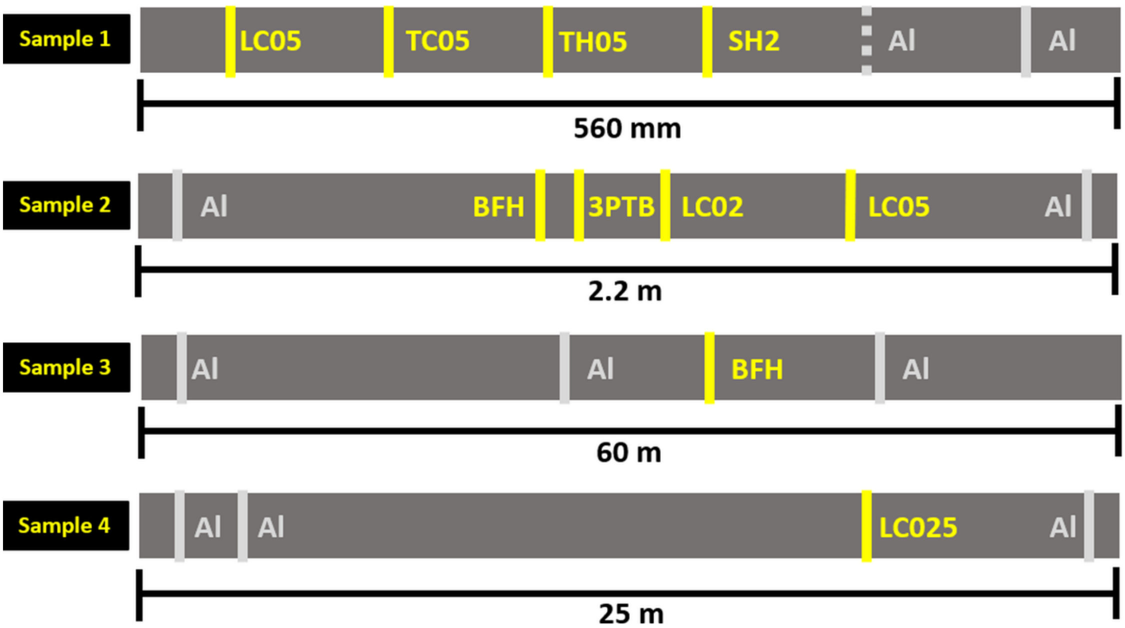

Fig. 4. Tested CFRP samples with the location of the defects.

3. Probe design

A set of functional requirements for the probes were defined in order to specify the inspection needs. The new customized probes should: i) have a high sensitivity to detect small defects with a very good signal-to-noise ratio when handled with conventional ECT equipment; ii) be capable of detecting distinct kinds of defects (morphology and locations); iii) provide the accurate position of the defect in Z direction; iv) be easily customizable and affordable. Four different probe geometries were designed, created and produced via Printed Circuit Board (PCB) technology on a rigid substrate (**Fig. 5**). This configuration was selected to maximize the proximity of all the winding to the surface of the CFRP and, hence, to the defect, allowing a superior sensitivity due to the proximity to the EC changes. PCB probes are also inexpensive to produce.

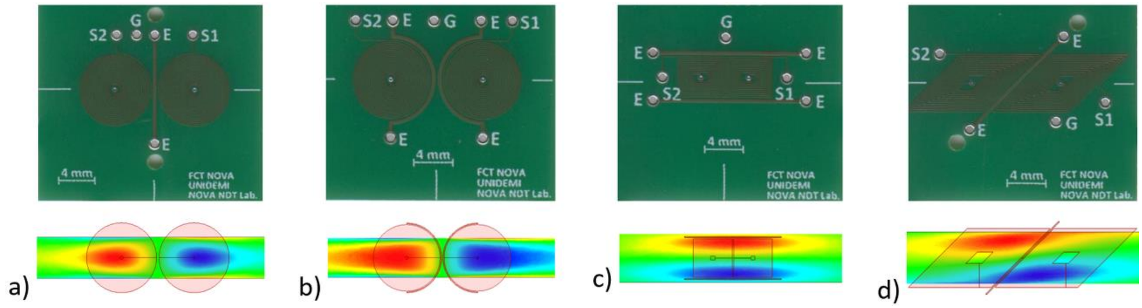

Fig. 5. PCB ECT probes designed and manufactured for testing with corresponding secondary magnetic field: a) Circular spiral coil probe with transversal excitation – Probe #1; b) Circular spiral coil probe with curved excitations – Probe #2; c) Rectangular spiral coil probe with parallel excitation – Probe #3; d) 45° parallelogram spiral coil probe with transverse excitation – Probe #4.

The probes consist of two planar pickup spiral coils and one or more excitation driver(s) tracks between them. The probe architecture is scalable to different widths according to the components to be inspected. Each of the probes can operate in two different modes. Reflection mode: using the middle track as a driver while the spiral pickup coils operate in differential mode. Using the same spiral coils, and ignoring the middle track in the probe, it can operate in bridge differential mode. Probe #1 uses planar circular spiral coils wound in opposition, and a rectilinear excitation filament placed in the symmetry plane, for reflection mode purposes (**Fig. 5a**). The secondary magnetic field, when operating in bridge mode, is also presented and it is possible to observe that the field is stronger under the sensing coils and spreads in the length direction of the CFRP. To decrease the distance between the excitation and the pickup spiral coils, Probe #2 was designed so that EC would be closer to the pickup coils (**Fig. 5b**) and will impose a more circular EC path. From the numeric simulation presented, while operating in reflection mode, it is possible to observe that the field is stronger and spreads more than with the previous probe. Probe #3 attempts to induce the EC in the direction of the fibres, with the two paths at the top and bottom of the pickup coils, and allows the current input in the same or opposite direction in these tracks, depending on the connection made (**Fig. 5c**). The secondary magnetic field, when operating in reflection mode, is displayed. The field spreads along the element near the edges and under the sensing coils. Probe #4 comprises of two 45° parallelogram spiral coils with a 45° excitation track in the middle (**Fig. 5d**). The secondary magnetic field, when operating in reflection mode, is spread at an angle under the sensing coils. The width of the parallelogram is the same as the CFRP element, maximizing the sensitive area, and either operating in reflection or bridge mode, the excitation is never transversal to the element as preferred considering the numeric simulation in **Fig. 3**. More numerical simulation results of the probes, where the EC density, EC vectors and secondary magnetic field for different operation modes, are shown in the supplementary data.

Probe #4 with dual 45° parallelogram spiral coils, was numerically simulated in order to assess its feasibility to inspect imperfections in the CFRP material. The probe operates in differential bridge mode with a 3 mm lift-off. The coils were simplified in order to decrease the number of elements required for the mesh and hence the simulation time (**Fig. 6a**). The parallelogram's outer dimensions are 5.7 mm width, 8 mm length and 35 μm thickness and it contains 12 turns (**Fig. 6b**). The model used for the simulation comprises only of one CFRP element and the respective probe. The CFRP element is modelled with the same section as the specimen, 5 × 2.5 mm, and 100 mm length. In **Fig. 7** is depicted the geometric model developed and the tetrahedral mesh representation which contains 2.7 million elements. The coils were excited with 1 A current at a frequency of 6 MHz. Two artificial defects were simulated. One was a top horizontal cut through the whole CFRP element with 0.5 mm thickness and depth as depicted in **Fig. 7a**. The other defect was a lateral cut through the whole element height also with 0.5 mm thickness and depth, as depicted in **Fig. 7**. **Fig. 8** depicts the EC density induced by the 45° parallelogram coils in the top surface of the element, where its behaviour around the defect can be seen.

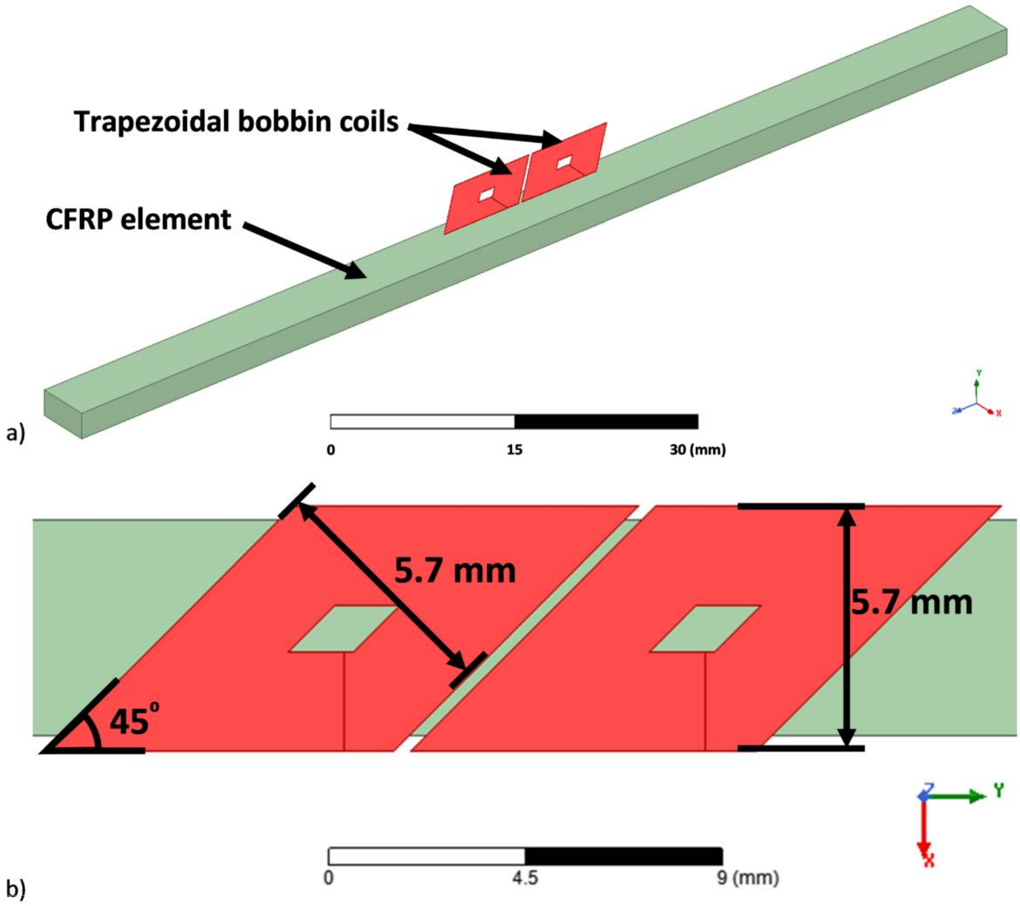

Fig. 6. Schematic representation of the model used for the probe simulation:
a) Isometric view of the element with the two coils; b) Top view of the coils and its dimensions.

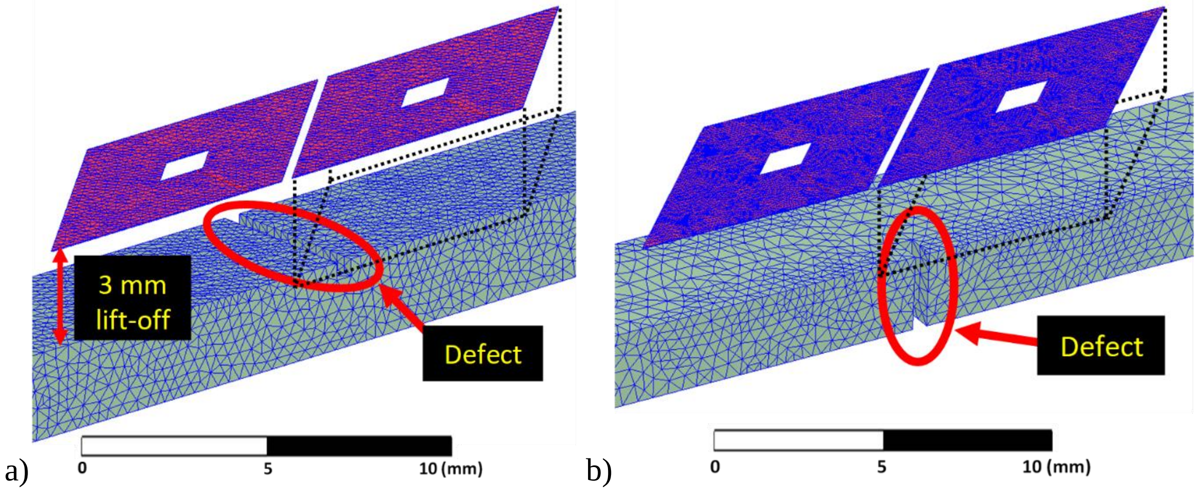

Fig. 7. Mesh representation with about 2.7 million tetrahedral elements:
a) With a top cross cut defect; b) With a lateral cut defect.

To simulate the inspection procedure, when the probe is scanning a defect, various defect positions along Z direction were simulated, keeping the probe at the same position. **Fig. 8** illustrates the EC density produced by the probe in one CFRP element, with the defect in three different positions, and its behaviour around the lateral cut defect. The output signal of the bobbins coils, in differential bridge operation, is shown in **Fig. 9**, where the blue line represents the output signal of the cross top cut defect, while the red line represents the side defect. According to the numerical simulations, both defects are detected with a clear output signal and with a good signal-to-noise ratio, especially the top cut defects. These signal outputs are the result of the compilation of the simulations performed with different defect positions. Each dot in **Fig. 9**, results from the simulation at that point and the defect is moved 500 μm between consecutive simulations. The distance was increased for probe positions longer than ± 15 mm away from the defect.

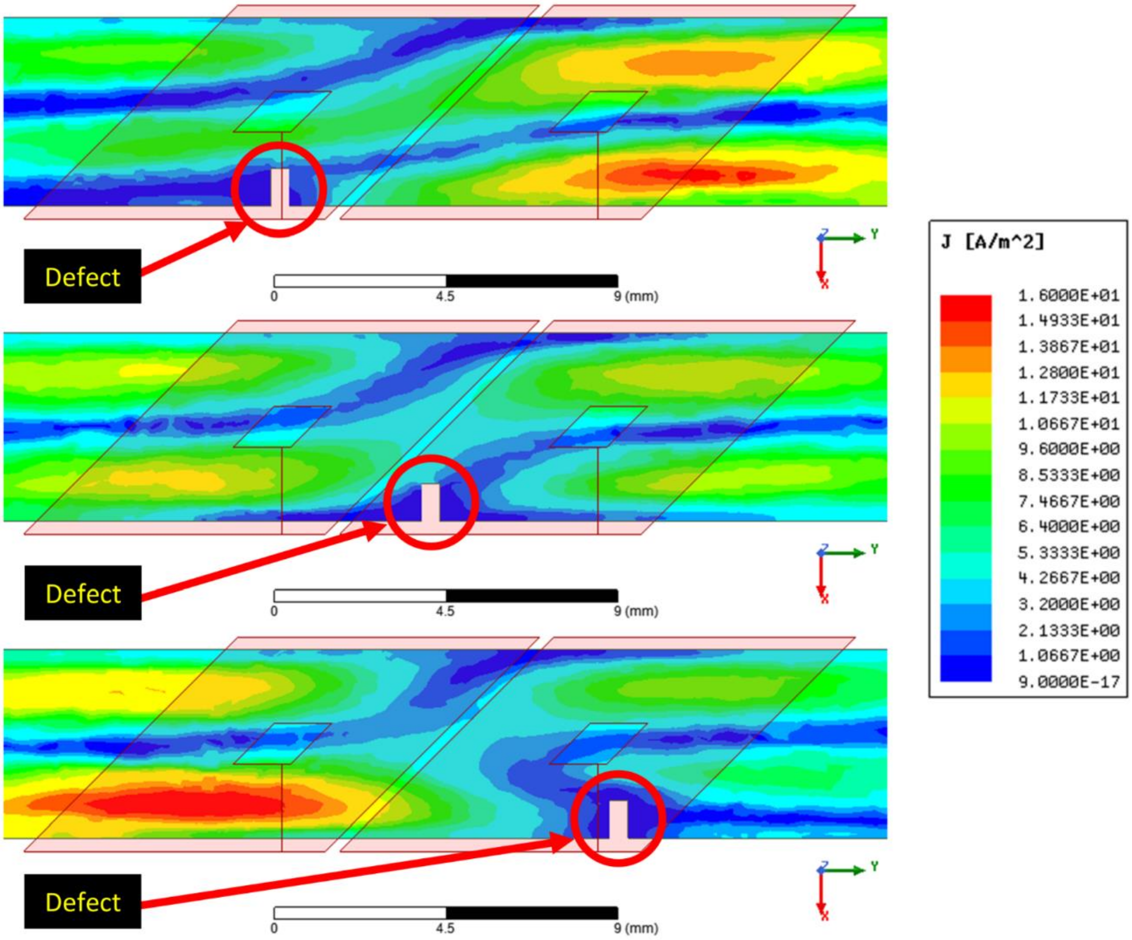

Fig. 8. Field of EC density on the top of the element with the lateral cut defect in three distinct positions.

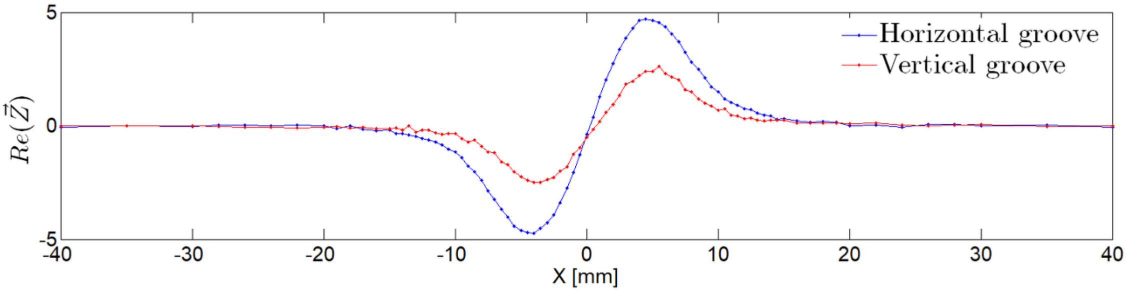

Fig. 9. Numerical simulated output signal of the parallelogram bridge differential probe of a top cross and lateral cut defect scanning.

Two array versions of Probe #4 were produced and tested to allow the inspection of the four CFRP elements simultaneously (**Fig. 10**). **Fig. 10a** shows the array version of Probe #4 with four individual 45° parallelogram spiral coils for the entire inspection the CFRP rope allowing monitoring each CFRP element separately but requiring four simultaneous impedance reading channels. **Fig. 10b** shows an array version that requires only two impedance channels for measuring two pairs of merged elements.

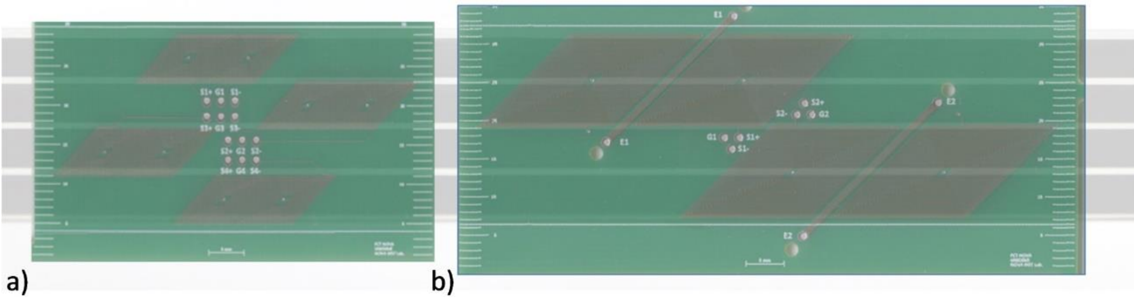

Fig. 10. Array versions of the Probe #4 with 45° parallelogram spiral coil overlapped with the four CFRP elements: a) Version with four individual coils; b) Version with two individual coils.

4. Experimental validation

In order to benchmark the tailored ECT probes, Sample 1 was inspected at low speed (20 mm/s). The experimental implementation was performed by means of an automated scanning device responsible for the CFRP movement while the probe remains stationary. The movement, as well as the signal acquisition, were controlled and programmed in LabVIEW environment and commercial ECT equipment (Nortec 500) was used for impedance measurements. **Fig. 11** shows the output signal from Sample 1 with the different ECT tailored probes with the best frequencies for each probe (all at 8 MHz except Probe #4 in bridge mode at 6 MHz). Regarding Probe #1, operating in bridge differential mode, the defect TH05 (drilled hole from the top), as well as the aluminum mark on the opposite side of the probe were not detected. This probe operating in reflection mode was not suitable due to the excitation track being too far away from the pickup coils. The second output signal corresponds to Probe #2 operating in reflection mode. Defects TH05, SH2 and the aluminum mark on the opposite side were not detected. The third output signal corresponds to Probe #3 operating in bridge differential mode. Reflection mode did not show any improvement. All the defects were detected except TH05. The fourth output signal corresponds to Probe #4 operating in reflection mode. All the defects were detected, except the aluminum mark on the opposite side of the inspection. The signal characteristic changed as well, since the "8" shape characteristic was lost, which means that the excitation does not induce currents under the whole sensing coils, only in the windings near the excitation track. The last output signal corresponds to Probe #4 operating in bridge differential mode at 6 MHz. All the defects were detected with a good signal-to-noise ratio. Probe #4 can detect all the defects because of its geometry. It induces the EC in the fibres preferential orientation as observed in the simulation. This maintains the EC pattern in the fibre as constant as possible in flawless fibres. So, when a fibre break occurs, a greater EC disturbance is created and measured by the probe.

Fig. 12 depicts the output signal of Probe #4 in an enlarged graph comparing to Ionic Probe [36] at 8 MHz, as well as, to a commercial ECT absolute pencil probe with 3 mm diameter with a fixed air-loaded reference coil in bridge mode at 6 MHz and a circular planar ECT absolute probe with 8 mm diameter with a fixed loaded reference coil over a good specimen in bridge mode at 6 MHz. Even though the defects are close to each other, all four defects and both aluminium marks are spotted by Probe #4 while the circular planar ECT absolute probe detected only three of them and the Ionic probe detected all but one with an inferior signal amplitude. On the other hand, the commercial probe managed to detect merely the top aluminium mark. This demonstrates the superior performance of planar PCB coils and the impact different geometries have for the same operation modes. The cut-like defects signal has a bigger amplitude than the through-hole defects.

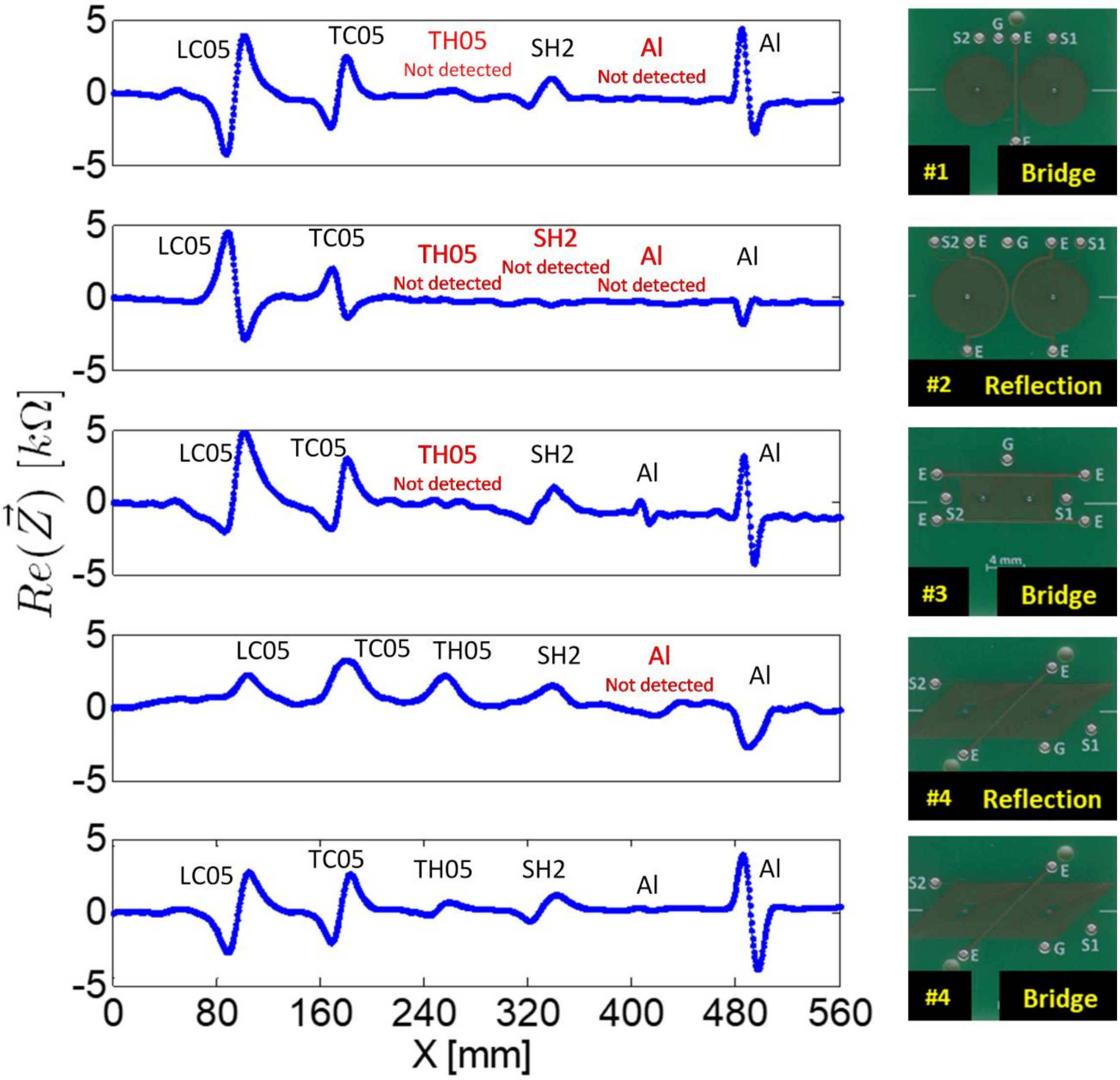

Fig. 11 Output signal of tailored ECT Probes inspecting the Sample 1 at low speed at 8 MHz, except Probe #4 in bridge mode at 6 MHz.

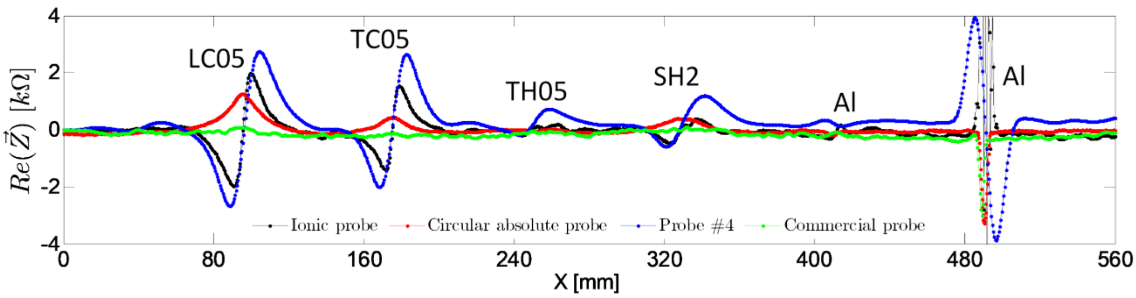

Fig. 12 Output signal of ECT Probe #4 inspecting the Sample 1 at 8 MHz at low speed comparing to the Ionic Probe at 8 MHz and commercially ECT absolute pencil probe with 3 mm diameter with a fixed air loaded reference coil in bridge mode at 6 MHz.

The most reliable tailored ECT probes were experimentally tested by means of an automated high-speed linear guide belt driven (1-4 m/s) responsible for the carbon fibre movement, while the probe remains stationary. Each one of the four CFRP elements was inspected one at a time. A 3D printed handheld chassis with two wheels was used for the high-speed tests (**Fig. 13)**. The probe is placed in the middle of the chassis and its positioning and constant lift off is assured by it. The wheels work like train wheels and the CFRP serves as the rail. This guarantees the transversal positioning of the probe relative to the CFRP.

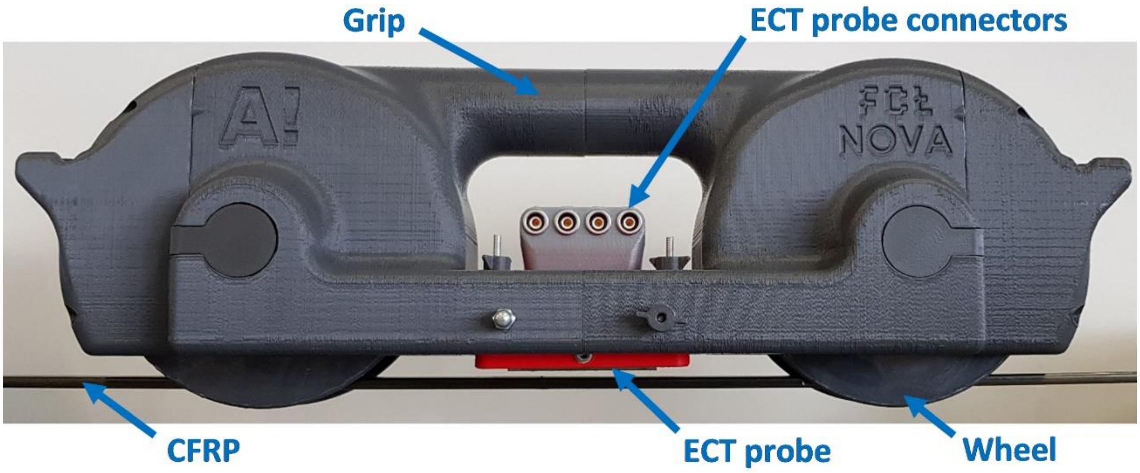

Fig. 13 Hand held device used in the high-speed tests.

A commercial GE Mentor EM impedance measure equipment was used. **Fig. 14** shows the output signal of Probe #4 operating in bridge differential mode at 6 MHz when inspecting CFRP Sample 2 at 3.5 m/s. The first and last differential signals were obtained from the aluminium markers that mark the beginning and the end of constant speed conditions. All four defects are clearly detected with excellent signal-to-noise ratio. As anticipated by the numerical simulations, top cut-like defects (BFH and 3PTB) produce signals with superior amplitude compared to lateral cut defects (LC02 and LC05). Zooming in on the lateral cut signals and overlapping with the numerical simulation results allows the comparison between them. **Fig. 15** and **Fig. 16** depict the experimental results (lateral cut LC05 and top cut 3PTB zoomed in, respectively) overlapping the numerical simulation results for the same defects. This provides an identification of the defect and they clearly agree in the exhibited trend.

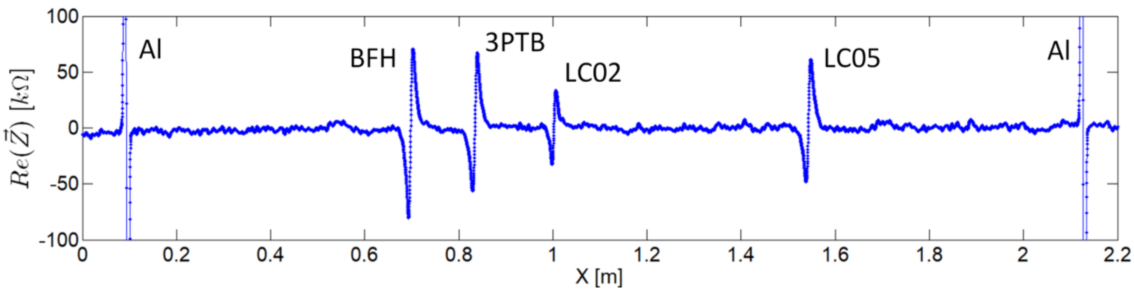

Fig. 14 Output signal of ECT Probe #4 operating in bridge differential mode inspecting Sample 2 at 6 MHz at 3.5 m/s.

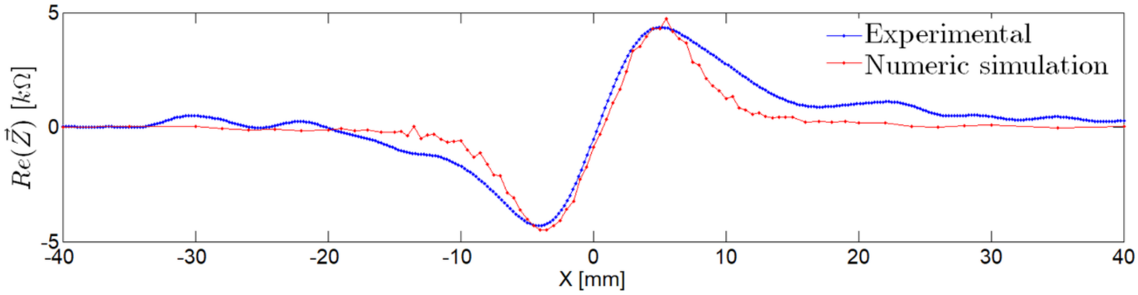

Fig. 15 Comparison between experimental results and numerical simulation by Finite Element Method (FEM) testing the lateral cut defect LC05 at 6 MHz and 3.5 m/s.

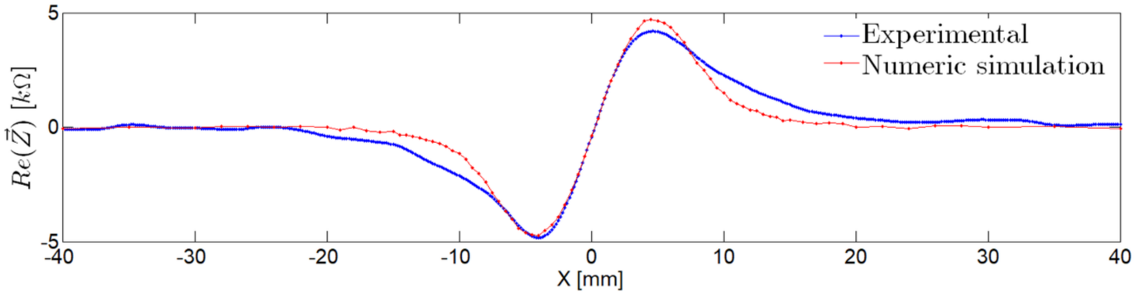

Fig. 16 Comparison between experimental results and numerical simulation by Finite Element Method (FEM) testing the cross top cut defect 3PTB at 6 MHz and 3.5 m/s.

Fig. 17 depicts the output signal of the array versions of Probe #4 with two 45° parallelogram spiral coils (**Fig. 10b**) operating in bridge differential mode at 6 MHz and inspecting Sample 2 at 3.5 m/s. In fact, since this probe inspects two elements with the same channel, the results correspond to two elements: one without defects and one that corresponds to Sample 2. All the defects are detected, but the signal amplitude has decreased, and the smallest lateral cut defect is barely noticeable. **Fig. 18** shows the output signal of Probe #4 inspecting Sample 2 at a velocity of 2 m/s, operating in reflection mode at 3 MHz. All the defects are distinguished although with an inferior signal-to-noise ratio. A commercial ECT absolute pencil probe with 3 mm diameter with a fixed air loaded reference coil in bridge mode at 6 MHz was tested in the same inspection conditions for comparison purposes, but only the aluminum strip marks were found (**Fig. 19**). This probe has a circular geometry which create and apply an axisymmetric magnetic field over the highly anisotropic CFRP material. Therefore, the EC generated are free spread along the fibre direction. This phenomenon increases the EC circulation area and, since the probe is small and can only measure what is beneath it, defect disturbance of EC outside this area cannot be detected.

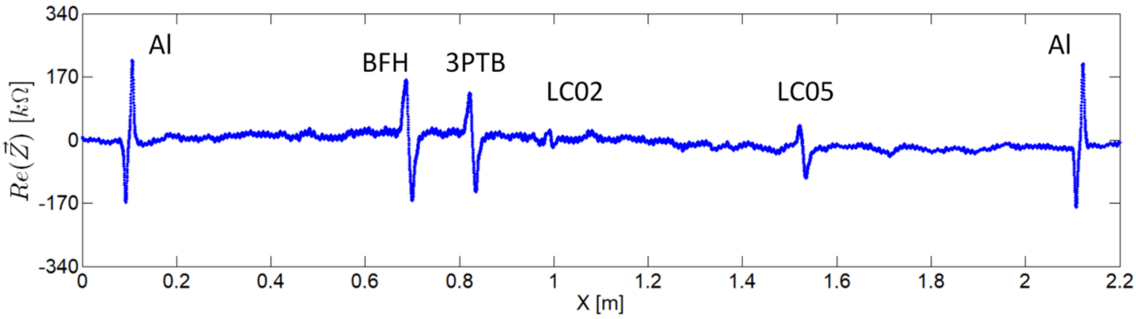

Fig. 17 Output signal of ECT Probe #4 (Fig. 10b) operating in bridge differential mode inspecting Sample 2 at 6 MHz at 3.5 m/s.

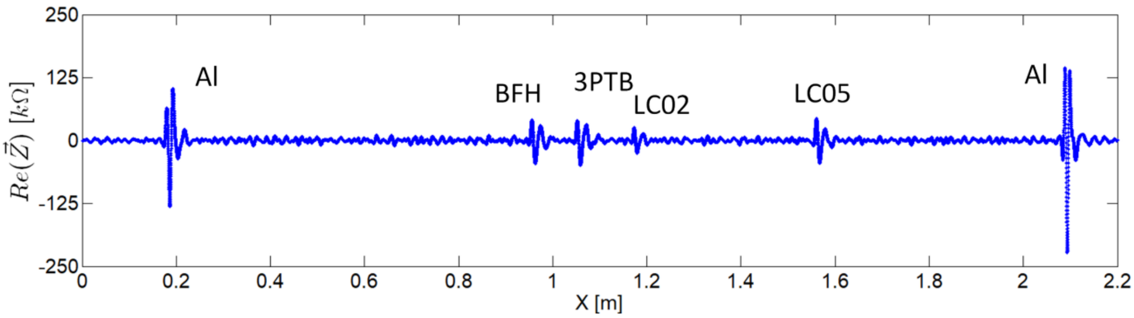

Fig. 18 Output signal of ECT Probe #4 operating in reflection mode inspecting Sample 2 at 3 MHz at 2 m/s.

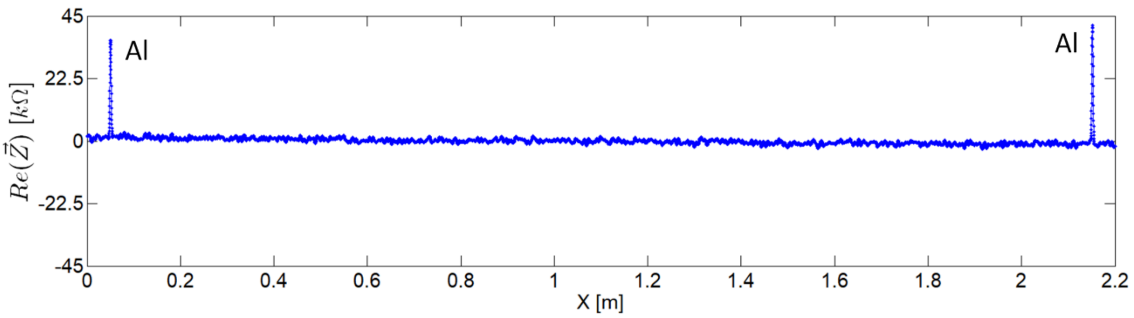

Fig. 19 Output signal of ECT commercial probe inspecting Sample 2 at 6 MHz at 2 m/s.

Fig. 20 shows the output signal of Probe #4 when inspecting Sample 3 at a velocity of 4 m/s operating in bridge differential mode at 6 MHz. The defect BFH is clearly detected with a good signal-to-noise ratio. **Fig. 21** illustrates the output signal of Probe #4 when inspecting Sample 4 at a velocity of 4 m/s operating in bridge differential mode at 6 MHz. The defect (LC025) is clearly detected with a good signal-to-noise ratio which characteristic signal can be seen zoomed in **Fig. 22**.

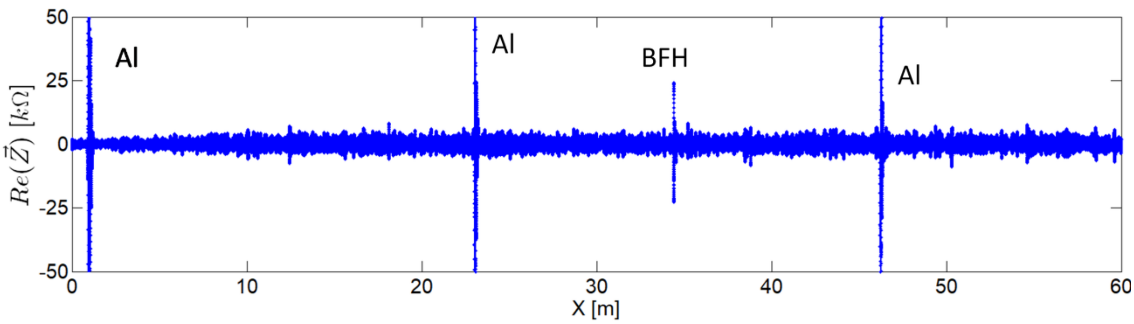

Fig. 20 Output signal of ECT Probe #4 inspecting Sample 3 at 6 MHz at 4 m/s.

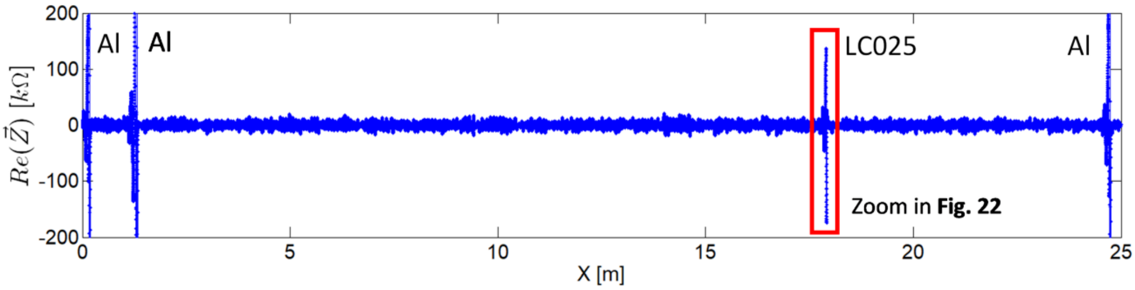

Fig. 21 Output signal of ECT Probe #4 inspecting Sample 4 at 6 MHz at 4 m/s.

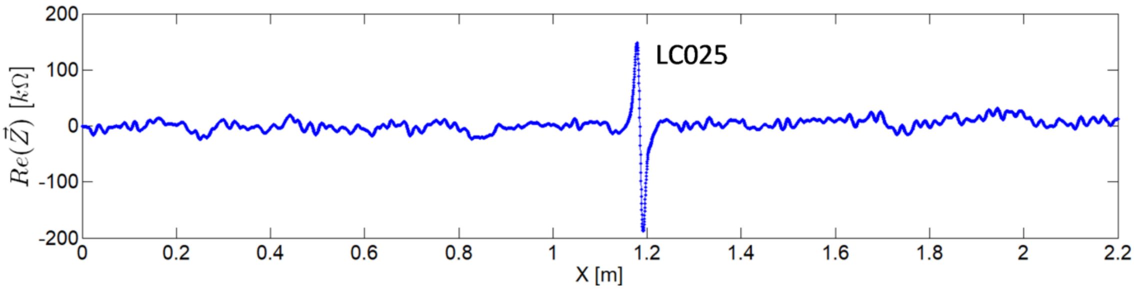

Fig. 22 Output signal of ECT Probe #4 inspecting Sample 4 at 6 MHz at 4 m/s zoomed in on the lateral cut defect.

5. Conclusions

This paper presented a tailored ECT probe solution for the health monitoring of a highly electrically anisotropic CFRP rope at high velocity and without contact. The main conclusions are:

Four tailored planar ECT probes were designed, manufactured and experimentally validated. These probes demonstrated superior performance when compared to commercial pencil probes or conventional circular spiral absolute probes. The four main features that contributed to this technological development were: the planar configuration which allows a closer proximity of all windings to the specimen; the size of the sensing coils which cover the full width of each CFRP element; the differential operation mode that allows a continuous comparison of two portions of the specimen; and the geometry of the coils itself are responsible for the EC and magnetic fields directions. These four features combined allowed a superior sensitivity of the ECT probes despite the high lift-off used.

The 45° parallelogram spiral coils probe demonstrated the best performance especially when operating in bridge differential mode at a frequency of 6 MHz. Speeds of 2-4 m/s were used in the CFRP inspections and the smallest lateral cuts (0.2 of the width) and fibre breaks were detected with a clear signal.

Using the PCB technology to produce the probes enabled a faster and consistent reproducibility and parametrization for different specimen dimensions.

Numerical simulations allowed better understanding of the EC behaviour in the CFRP component and thus were an essential tool in assisting the probe design. The experimental results were consistent with the numerical simulations performed. It was also understood from the simulations, and confirmed experimentally, that the probes are not able to detect defects on the other side of the CFRP since, although there are currents flowing there, there is not a sensor to sense the local EC deviations. Future work will focus on an integral CFRP inspection (both sides) and different defects like delamination.

Acknowledgements

MAM would like to acknowledge Fundação para a Ciência e a Tecnologia (FCT-MCTES) for its financial support via the PhD scholarship FCT-SFRH/BD/108168/2015. TGS acknowledge FCT-MCTES for the financial support in the scope of PEst-OE/EME/UI0667/2014 (UNIDEMI). KNA acknowledge the Finnish Funding Agency for Technology and Innovation (TEKES).

References

[1] Sarasini F, Tirillò J, D'Altilia S, Valente T, Santulli C, Touchard F, et al. Damage tolerance of carbon/flax hybrid composites subjected to low velocity impact. Compos Part B Eng 2016;91:144–53. doi:10.1016/j.compositesb.2016.01.050.

[2] Wang S-X, Wu L-Z, Ma L. Low-velocity impact and residual tensile strength analysis to carbon fiber composite laminates. Mater Des 2010;31:118–25. doi:10.1016/j.matdes.2009.07.003.

[3] Gholizadeh S. A review of non-destructive testing methods of composite materials. Procedia Struct Integr 2016;1:50–7. doi:10.1016/j.prostr.2016.02.008.

[4] Schumacher D, Antin K-N, Zscherpel U, Vilaça P. Application of Different X-ray Techniques to Improve In-Service Carbon Fiber Reinforced Rope Inspection. J Nondestruct Eval 2017;36:62. doi:10.1007/s10921-017-0441-5.

[5] Antin KN, Harhanen L, Bossuyt S. Damage detection in CFRP components using DIC. Conf. Proc. Soc. Exp. Mech. Ser., vol. 3, 2016, p. 57–62. doi:10.1007/978-3-319-22446-6_7.

[6] Patsias S, Staszewski WJ, Tomlinson GR. Image sequences and wavelets for vibration analysis: Part 1: Edge detection and extraction of natural frequencies. Proc Inst Mech Eng Part C J Mech Eng Sci 2002;216:885–900. doi:10.1177/095440620221600903.

[7] Brönnimann R, Nellen PM, Sennhauser U. Application and reliability of a fiber optical surveillance system for a stay cable bridge. Smart Mater Struct 1998;7:229–36. doi:10.1088/0964-1726/7/2/010.

[8] Mukherjee S, Tamburrino A, Haq M, Udpa S, Udpa L. Far field microwave NDE of composite structures using time reversal mirror. NDT E Int 2018;93:7–17. doi:10.1016/j.ndteint.2017.09.008.

[9] Park JB, Okabe T, Takeda N, Curtin WA. Electromechanical modeling of unidirectional CFRP composites under tensile loading condition. Compos Part A Appl Sci Manuf 2002;33:267–75. doi:10.1016/S1359-835X(01)00097-5.

[10] Kupke M, Schulte K, Schüler R. Non-destructive testing of FRP by d.c. and a.c. electrical methods. Compos Sci Technol 2001;61:837–47. doi:10.1016/S0266-3538(00)00180-9.

[11] Todoroki A. Monitoring of electric conductance and delamination of CFRP using multiple electric potential measurements. Adv Compos Mater 2014;23:179–93. doi:10.1080/09243046.2013.844900.

[12] Abry J., Choi Y., Chateauminois A, Dalloz B, Giraud G, Salvia M. In-situ monitoring of damage in CFRP laminates by means of AC and DC measurements. Compos Sci Technol 2001;61:855–64. doi:10.1016/S0266-3538(00)00181-0.

[13] Cheng J, Qiu J, Xu X, Ji H, Takagi T, Uchimoto T. Research advances in eddy current testing for maintenance of carbon fiber reinforced plastic composites. Int J Appl Electromagn Mech 2016;51:261–84. doi:10.3233/JAE-150168.

[14] Heuer H, Schulze M, Pooch M, Gäbler S, Nocke A, Bardl G, et al. Review on quality assurance along the CFRP value chain – Non-destructive testing of fabrics, preforms and CFRP by HF radio wave techniques. Compos Part B Eng 2015;77:494–501. doi:10.1016/j.compositesb.2015.03.022.

[15] Hughes RR, Drinkwater BW, Smith RA. Characterisation of carbon fibre-reinforced polymer composites through radon-transform analysis of complex eddy-current data. Compos Part B Eng 2018;148:252–9. doi:10.1016/j.compositesb.2018.05.007.

[16] Bouloudenine A, Feliachi M, Latreche MEH. Development of circular arrayed eddy current sensor for detecting fibers orientation and in-plane fiber waviness in unidirectional CFRP. NDT E Int 2017;92:30–7. doi:10.1016/j.ndteint.2017.07.011.

[17] Cheng J, Ji H, Qiu J, Takagi T, Uchimoto T, Hu N. Role of interlaminar interface on bulk conductivity and electrical anisotropy of CFRP laminates measured by eddy current method. NDT E Int 2014;68:1–12. doi:10.1016/j.ndteint.2014.07.001.

[18] Xu X, Ji H, Qiu J, Cheng J, Wu Y, Takagi T. Interlaminar contact resistivity and its influence on eddy currents in carbon fiber reinforced polymer laminates. NDT E Int 2018;94:79–91. doi:10.1016/j.ndteint.2017.12.003.

[19] Mook G, Lange R, Koeser O. Non-destructive characterisation of carbon-fibre-reinforced plastics by means of eddy-currents. Compos Sci Technol 2001;61:865–73. doi:10.1016/S0266-3538(00)00164-0.

[20] Cheng J, Qiu J, Ji H, Wang E, Takagi T, Uchimoto T. Application of low frequency ECT method in noncontact detection and visualization of CFRP material. Compos Part B Eng 2017;110:141–52. doi:10.1016/j.compositesb.2016.11.018.

[21] Gros XE, Takahashi K. Monitoring Delamination Growth In Cfrp Materials Using Eddy Currents. Nondestruct Test Eval 1998;15:65–82. doi:10.1080/10589759908952865.

[22] Vertuccio L, Guadagno L, Spinelli G, Lamberti P, Zarrelli M, Russo S, et al. Smart coatings of epoxy based CNTs designed to meet practical expectations in aeronautics. Compos Part B Eng 2018;147:42–6. doi:10.1016/j.compositesb.2018.04.027.

[23] Spinelli G, Lamberti P, Tucci V, Vertuccio L, Guadagno L. Experimental and theoretical study on piezoresistive properties of a structural resin reinforced with carbon nanotubes for strain sensing and damage monitoring. Compos Part B Eng 2018;145:90–9. doi:10.1016/j.compositesb.2018.03.025.

[24] Ryosi A, Valentino M, Peluso G, Pepe G. Analysis of low-velocity impact damage in reinforced carbon fiber composites by HTS-SQUID magnetometers. IEEE Trans Appiled Supercond 2001;11:1172–5. doi:10.1109/77.919557.

[25] Placko D, Dufour I. Eddy current sensors for nondestructive inspection of graphite composite materials. Conf Rec 1992 IEEE Ind Appl Soc Annu Meet n.d.:1676–82.

doi:10.1109/IAS.1992.244235.

[26] Machado MA, Rosado L, Pedrosa N, Vostner A, Miranda RM, Piedade M, et al. Novel eddy current probes for pipes: Application in austenitic round-in-square profiles of ITER. NDT E Int 2017;87:111–8. doi:10.1016/j.ndteint.2017.02.001.

[27] Rosado LS, Santos TG, Ramos PM, Vilaça P, Piedade M. A new dual driver planar eddy current probe with dynamically controlled induction pattern. NDT E Int 2015;70:29–37. doi:10.1016/j.ndteint.2014.09.009.

[28] Machado MA, Rosado L, Pedrosa N, Miranda RM, Piedade M, Santos TG. Customized Eddy Current Probes for Pipe Inspection. Stud Appl Electromagn Mech 2017;42:283–90. doi:10.3233/978-1-61499-767-2-283.

[29] Koyama K, Hoshikawa H. Influence of Speed Effect in Eddy Current Nondestructive Testing. Nondestruct Test Eval 1992;7:73–82. doi:10.1080/10589759208952989.

[30] Ida N. Modeling of velocity effects in eddy current applications. J Appl Phys 1988;63:3007–9. doi:10.1063/1.340929.

[31] Rocha TJ, Ramos HG, Lopes Ribeiro A, Pasadas DJ. Magnetic sensors assessment in velocity induced eddy current testing. Sensors Actuators A Phys 2015;228:55–61. doi:10.1016/j.sna.2015.02.004.

[32] Kwon D-J, Kim J-H, Park S-M, Kwon I-J, DeVries KL, Park J-M. Damage sensing, mechanical and interfacial properties of resins suitable for new CFRP rope for elevator applications. Compos Part B Eng 2019;157:259–65. doi:10.1016/j.compositesb.2018.08.049.

[33] Yarn testing. Suragus Sensors & Instruments 2018. https://www.suragus.com (accessed October 31, 2018).

[34] Bardl G, Nocke A, Hübner M, Gereke T, Pooch M, Schulze M, et al. Analysis of the 3D draping behavior of carbon fiber non-crimp fabrics with eddy current technique. Compos Part B Eng 2018;132:49–60. doi:10.1016/j.compositesb.2017.08.007.

[35] Miranda RM, Gandra JP, Vilaca P, Quintino L, Santos TG. Surface modification by solid state processing. Surf. Modif. by Solid State Process., 2014, p. 1–183. doi:10.1533/9780857094698.

[36] Rosado LS, Gonzalez JC, Santos TG, Ramos PM, Piedade M. Geometric optimization of a differential planar eddy currents probe for non-destructive testing. Sensors Actuators A Phys 2013;197:96–105. doi:10.1016/j.sna.2013.04.010.